nature nanotechnology

LETTERS

PUBLISHED ONLINE: 11 JULY 2016 | DOI: 10.1038/NNANO.2016.112

Quantum interference in an interfacial superconductor

Srijit Goswami[1*†], Emre Mulazimoglu[1†], Ana M. R. V. L. Monteiro[1], Roman Wölbing[2], Dieter Koelle[2], Reinhold Kleiner[2], Ya. M. Blanter[1], Lieven M. K. Vandersypen[1] and Andrea D. Caviglia[1*]

The two-dimensional superconductor that forms at the interface between the complex oxides lanthanum aluminate (LAO) and strontium titanate (STO)[1] has several intriguing properties[2–6] that set it apart from conventional superconductors. Most notably, an electric field can be used to tune its critical temperature (T_c; ref. 7), revealing a dome-shaped phase diagram reminiscent of high-T_c superconductors[8]. So far, experiments with oxide interfaces have measured quantities that probe only the magnitude of the superconducting order parameter and are not sensitive to its phase. Here, we perform phase-sensitive measurements by realizing the first superconducting quantum interference devices (SQUIDs) at the LAO/STO interface. Furthermore, we develop a new paradigm for the creation of superconducting circuit elements, where local gates enable the *in situ* creation and control of Josephson junctions. These gate-defined SQUIDs are unique in that the entire device is made from a single superconductor with purely electrostatic interfaces between the superconducting reservoir and the weak link. We complement our experiments with numerical simulations and show that the low superfluid density of this interfacial superconductor results in a large, gate-controllable kinetic inductance of the SQUID. Our observation of robust quantum interference opens up a new pathway to understanding the nature of superconductivity at oxide interfaces.

A SQUID consists of two Josephson junctions (JJs) embedded in a superconducting loop. When a magnetic flux (Φ) threads through this loop, it changes the relative difference in the superconducting phase of the two JJs giving rise to periodic oscillations in the supercurrent. This basic principle has been used with great success to study a variety of material systems. For example, standard superconductors have been combined with other materials such as ferromagnets[9,10], topological insulators[11] and nanowires[12] to often reveal non-trivial current-phase relations. Such phase-sensitive measurements have also emerged as a powerful tool to study more exotic superconductors such as the ruthenates[13] and high-T_c cuprates[14]. Whether the 2D superconductor formed at the LAO/STO interface is also unconventional is still not clear. However, to address this issue one must move beyond standard bulk transport measurements. Recent tunnelling studies[8] and transport spectroscopy of confined structures[15] exemplify this point. In this context, a probe of the superconducting phase could provide complementary information about the microscopic origin of the superconductivity, but such experiments have not yet been undertaken. To address this, we realize SQUIDs at the LAO/STO interface that enable the observation of robust quantum interference in this interfacial superconductor.

We fabricate the SQUIDs using two distinct approaches (see the Supplementary Information for full details). The first involves the creation of weak links using nanoscale physical constrictions (C-SQUIDs), a technique that has been used extensively in a wide variety of superconductors. Figure 1a shows a schematic of the C-SQUID. Black areas are superconducting, whereas the beige regions remain insulating due to the presence of an amorphous LAO (a-LAO) mask. Each arm of the loop is interrupted by a narrow constriction (see the AFM image in Fig. 1b). We ensure that the width of the constriction (<100 nm) is less than/comparable to the superconducting coherence length of LAO/STO[1]. The C-SQUID has the advantage that it requires only a single lithography step and is simple to characterize.

The second approach used to define SQUIDs, although more involved, is novel and unique to the LAO/STO interface. We exploit the sensitivity of T_c to the field effect to create an electrostatically defined SQUID (E-SQUID). By applying negative voltages to the local top gates (see schematic in Fig. 1c), we deplete the regions below them. These locally depleted regions serve as the weak links, thus enabling the formation of independently tunable JJs in each arm. Figure 1d shows an AFM image of one such gate-defined JJ. Although other examples of gate-tunable JJs do exist[16–18], they necessarily involve physical interfaces between two dissimilar materials. In contrast, LAO/STO provides a unique material platform in which a single superconductor can be electrostatically modified to allow the *in situ* creation and tuning of JJs in a perfectly reversible manner. In this work we study two C-SQUID devices (C-SQ1 and C-SQ2) and one E-SQUID device (E-SQ3). A back gate can be used to tune the global electronic properties of the devices and measurements are performed in a dilution refrigerator with a base temperature of 40 mK.

Figure 1e shows a voltage–current (V–I) curve for C-SQ1 at 40 mK, which displays a distinct supercurrent branch (the inset shows the measurement configuration). To establish the presence of Josephson coupling we test whether the devices show clear SQUID behaviour. We apply a current bias close to the critical current (I_c) and monitor the voltage drop as a function of the perpendicular magnetic field (B). Figure 1f shows that all of the devices undergo periodic oscillations in B. As we expect these oscillations to be periodic in the flux threading through the SQUID, a reduction in the loop area should result in a larger period in B. This is precisely what we observe when we compare C-SQ1 (upper panel) and C-SQ2 (middle panel), where C-SQ2 is designed to have a smaller loop area. E-SQ3 also shows similar periodic oscillations (lower panel) when the top gates are appropriately tuned (discussed in more detail below). The period (ΔB) for each of the traces in Fig. 1f can be determined by Fourier analysis (Fig. 1g) to be 19 μT,

[1]Kavli Institute of Nanoscience, Delft University of Technology, PO Box 5046, 2600 GA Delft, The Netherlands. [2]Physikalisches Institut and CQ Center for Quantum Science in LISA[+], Eberhard Karls Universität Tübingen, Auf der Morgenstelle 14, D-72076 Tübingen, Germany. †These authors contributed equally to this work. *e-mail: s.goswami@tudelft.nl; a.caviglia@tudelft.nl

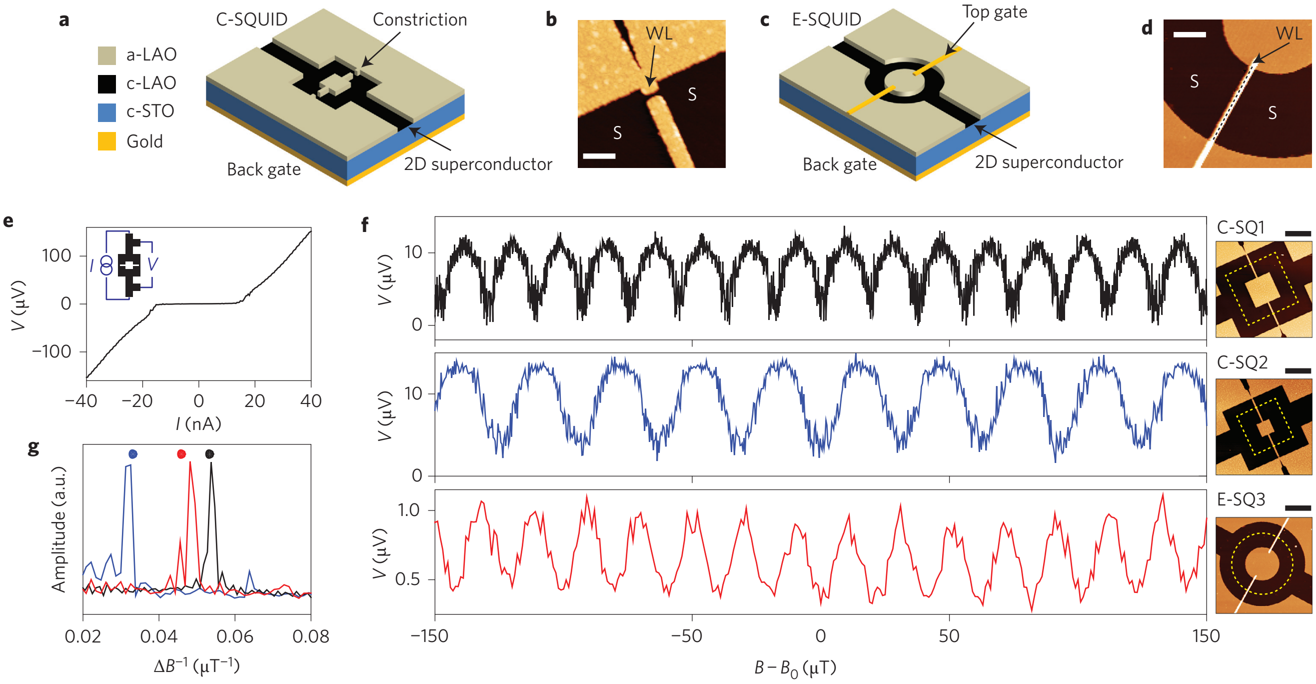

Figure 1 | Device description and $V(\Phi)$ oscillations. a, Schematic of the C-SQUID. **b**, AFM image of the constriction, which serves as the weak link (WL). Scale bar, 400 nm. **c**, Schematic of the E-SQUID. **d**, AFM image of the region around the top gate. Scale bar, 2 μm. The dashed line shows the region below the gate where the WL forms when a negative gate voltage is applied to the gate. **e**, V–I curve for C-SQ1 at $V_{bg} = -7$ V. Inset: Schematic of the measurement configuration. **f**, Oscillations in V with magnetic field ($B - B_0$) for C-SQ1 (upper panel), C-SQ2 (middle panel) and E-SQ3 (lower panel) with AFM images of the respective devices. Scale bars, 5 μm. B_0 is an experimentally determined offset in the magnetic field and has an uncertainty greater than one oscillation period. The yellow dashed lines in the AFM images mark the effective area threaded by the flux. **g**, Fourier transform of the oscillations shown in **f** (the colour scheme is the same as in **f**). The circles are results of numerical simulations that yield an oscillation period in close agreement with the experiments.

31 μT and 21 μT for C-SQ1, C-SQ2 and E-SQ3, respectively. This gives us an effective loop area $A_{eff} = \Phi_0/\Delta B$ ($\Phi_0 = h/2e$ is the flux quantum, h is Planck's constant, and e is the electron charge), which is consistently larger than the lithographically defined central (insulating) area. For superconducting structures that are much larger than the magnetic field penetration depth this difference arises from the Meissner effect in the superconducting region, which focuses the applied field into the centre of the SQUID loop. Even for 2D SQUIDs with dimensions smaller than the penetration depth (Pearl length) the fluxoid quantization can lead to a large flux-focusing effect[19]. We confirm this via numerical simulations of the 2D current distributions in thin-film superconductors[20], which include the (weak) Meissner effect of the shielding currents (see the Supplementary Information for details of the simulations and flux-focusing factors). Taking into account the exact geometry of the devices, we find that the calculated periods (circles in Fig. 1g) agree well with the experiments.

Although the $V(\Phi)$ oscillations clearly demonstrate the successful creation of SQUIDs at the LAO/STO interface, analysis of $I_c(\Phi)$ oscillations provides a more quantitative understanding of the factors that determine the SQUID response. In the absence of thermal fluctuations the maximum critical current (I_{max}) across the SQUID is set by the Josephson coupling energy and the minimum critical current (I_{min}) is determined by the screening parameter $\beta_L = I_{max}L/\Phi_0$ (where L is the total inductance of the SQUID loop). In other words L plays a crucial role in determining the visibility, Vis $= (I_{max} - I_{min})/I_{max}$, of the $I_c(\Phi)$ oscillations. The exact relation between Vis and β_L can be obtained by numerical simulations (see the red curve in Fig. 2c). To experimentally determine Vis, we keep the back gate voltage (V_{bg}) fixed and record V–I curves for different values of Φ (Fig. 2a) to estimate I_{max} and I_{min} (Fig. 2b). We find that for $V_{bg} = 4$V, $I_{max} = 88$nA and Vis ~ 0.3. From Fig. 2c we estimate β_L to be 2.1, giving $L \approx 50$ nH. This is nearly three orders of magnitude larger than the estimated geometric inductance of the SQUID loop. This additional inductance of the superconductor arises from the kinetic energy stored in the Cooper pairs and is known as the kinetic inductance (L_k). In general it can be expressed as $L_k \propto (m^*/n_s d)$, where m^* is the effective mass of the charge carriers, n_s is the superfluid density and d is the thickness of the superconductor. The 2D nature of the LAO/STO interface ($d \approx 10$ nm)[21], combined with an extremely low n_s value[22] and large m^* value[23] naturally result in a greatly enhanced L_k. Although for most SQUID designs the contribution of L_k can be neglected, here the SQUID response is in fact dominated by L_k. Thus, an analysis of the $I_c(\Phi)$ oscillations, as described above, allows us to estimate the L_k of our SQUID loop.

Figure 2d shows that the kinetic inductance of the SQUID can be continuously tuned with the back gate (see the Supplementary Information for details of the analysis and error estimates). To our knowledge this is the only intrinsic superconductor where the kinetic inductance can be tuned *in situ* via the field effect. Increasing V_{bg} induces more carriers at the LAO/STO interface which in turn increases the superfluid density[22]. This results in an overall decrease in L_k. In addition to the back gate voltage, we expect the temperature to also have a substantial effect on L_k. Increasing the temperature should reduce n_s, thereby increasing L_k. Indeed, Fig. 2e clearly shows that L_k increases with temperature. We therefore find that both the back gate and temperature dependence of L_k are mutually consistent with the picture that the SQUID modulations are determined predominantly by the kinetic inductance. We compare our results in Fig. 2e with numerical simulations, solving the London equations for our geometry[20]. Using the Ginzburg–Landau expression for the London penetration depth $\lambda_L(T) = \lambda_L(0)/(1 - T/T_c)^{1/2}$ (ref. 24) and the experimentally

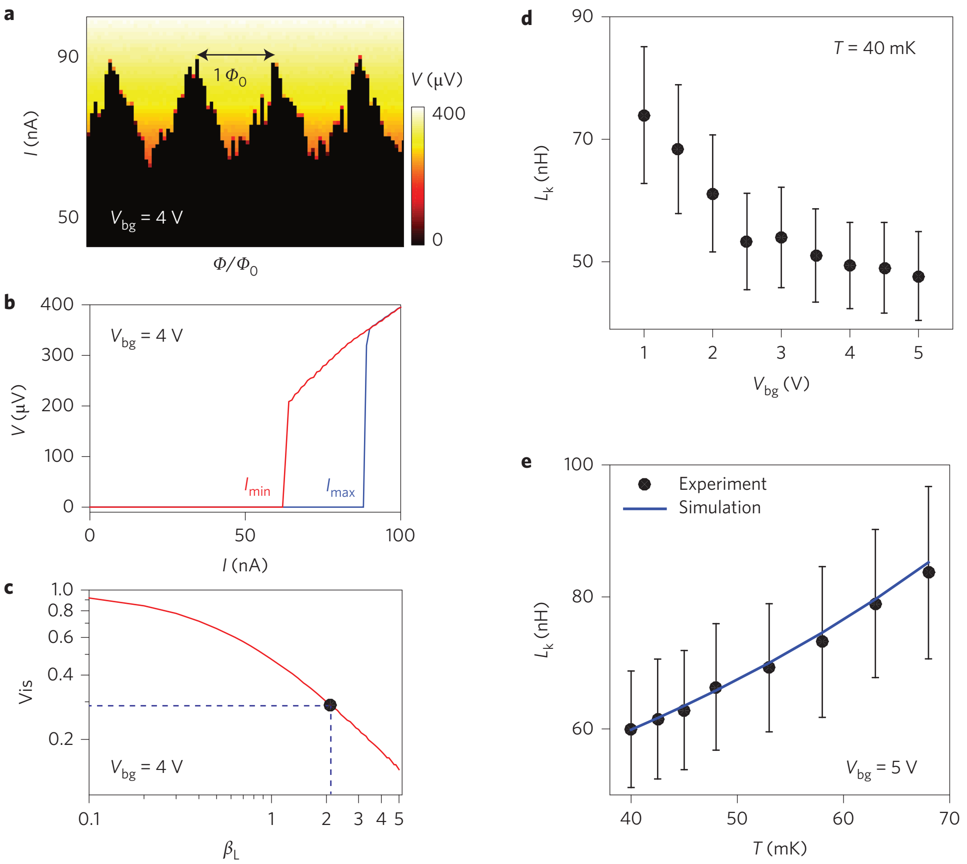

Figure 2 | $I(\Phi)$ oscillations and kinetic inductance in C-SQUIDs. a, Colour maps of V–I curves for different values of the normalized flux (Φ/Φ_0) at $V_{bg} = 4$ V. **b**, Individual V–I traces from **a** showing I_{max} and I_{min}. **c**, Numerically simulated curve (red) for Vis versus β_L in the noise-free case with the experimentally obtained value of Vis (black circle) at $V_{bg} = 4$ V. **d**, Variation of L_k with V_{bg}. **e**, Variation of L_k with temperature at $V_{bg} = 5$ V (black circles) in comparison with numerical simulations (blue curve). These measurements were performed in a different cool-down, resulting in a slightly different value of L_k than in **d**.

determined $T_c = 213$ mK, we find a good agreement between the experiments and simulations (blue curve). For the Pearl length $\Lambda_P(T) = 2\lambda_L(T)^2/d$ we obtain a value of 3 mm at $T = 40$ mK, which is similar in magnitude to the value obtained via scanning SQUID measurements[22]. Furthermore, we find that L_k is dominated by the constrictions, which behave as quasi-1D structures connected to the 2D bulk superconducting reservoirs (see the Supplementary Information for a full description of the calculations).

The C-SQUIDs describe a simple yet effective way to demonstrate quantum interference at the LAO/STO interface. However, they do not allow one to locally control the weak links. In contrast the E-SQUID (described earlier, see Fig. 1c,d) uses local top gates to create and control JJs in each arm of the SQUID. Although some previous studies with a single top gate have shown evidence of a gate controllable Josephson effect[25–27], there was no clear observation of quantum interference. We now describe the operation of the E-SQUID in detail. When no gate voltages are applied to either of the gates ($V_l = V_r = 0$ V) the device is equivalent to a simple superconducting loop. The black trace in Fig. 3a shows the corresponding V–I trace. When a large negative voltage is applied only to the left gate $V_l = -3.4$ V the current flow through the left arm decreases, thereby reducing the total critical current across the loop (green trace). The red trace shows a similar V–I curve when only the right gate is made highly negative ($V_r = -3.8$ V) (refer to the Supplementary Information for more details about the tuning procedure). As expected, none of these three electrostatic configurations produce SQUID oscillations. However, when both gates are depleted ($V_l = -3.4$ V and $V_r = -3.8$ V, blue trace) I_c reduces significantly. Figure 3b shows the V–I trace in this gate configuration over a smaller range. Here we observe distinct SQUID oscillations (Fig. 3c), thereby demonstrating the existence of an electrostatically defined JJ in each of the arms. We note that this process is completely reversible, whereby removing the gate voltages brings the device back to its original state, with no JJs.

The sensitivity of the JJs to the top gate voltages defines an optimal operating range for the E-SQUID. To quantify this we keep the right gate fixed at $V_r = -3.8$ V and monitor the visibility for different values of V_l, as shown in Fig. 3d–g. The left inset shows the voltages applied to the left/right gates (these measurements were performed during a different cool-down from the ones described in Fig. 3a–c, and therefore the absolute values of the voltages are somewhat different). When the left gate is relatively open (Fig. 3d) the oscillations are hardly visible (Vis ~ 0). As V_l is made more negative the visibility increases, reaching a maximum value of 0.3 (Fig. 3f). By depleting the region below the left gate even further, the oscillations disappear again. This continuous transition can be physically understood as follows. As the top gates act locally, their influence on the superconducting banks is minimal. Therefore the maximum visibility is obtained when both JJs have the same critical current. This condition is satisfied for Fig. 3f ($V_r = -3.8$ V, $V_l = -2.9$ V). Tuning V_l away from this optimal condition thus increases the asymmetry between the two JJs resulting in a reduced visibility.

For SQUIDs with a small loop inductance the dominant source of asymmetry arises due to unequal values of critical current in the two JJs (that is, $I_{cl} \neq I_{cr}$, see SQUID schematic in inset to Fig. 4c). On the other hand, when L_k is large (as is the case for LAO/STO) one must consider the combined effects of asymmetries in I_c and L_k in

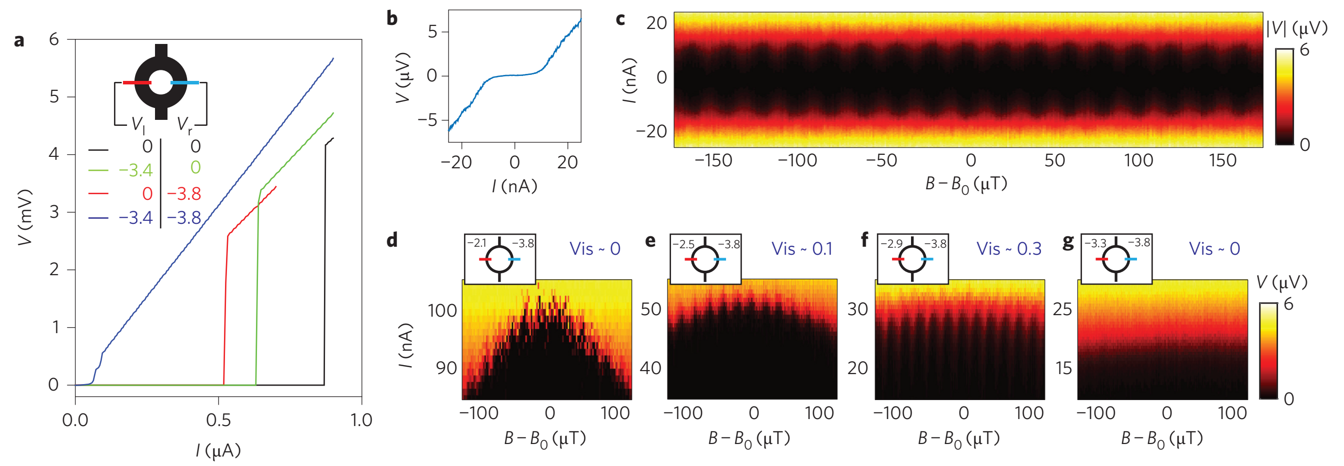

Figure 3 | Tunable Josephson junctions in E-SQUIDs. **a**, V–I curves for different combinations of V_l and V_r with $V_{bg} = -1$ V. Inset: Schematic of the device. **b**, Zoom-in of the blue trace in **a**. **c**, 2D plot showing SQUID oscillations with the top gates optimally tuned ($V_l = -3.4$ V, $V_r = -3.8$ V). **d–g**, Variation in the visibility of the modulations as V_l is reduced, with V_r held constant. The values of V_l and V_r for each panel are indicated in the left inset. These measurements were performed during a different cool-down as compared with **a–c**, resulting in slightly different values of gate voltages.

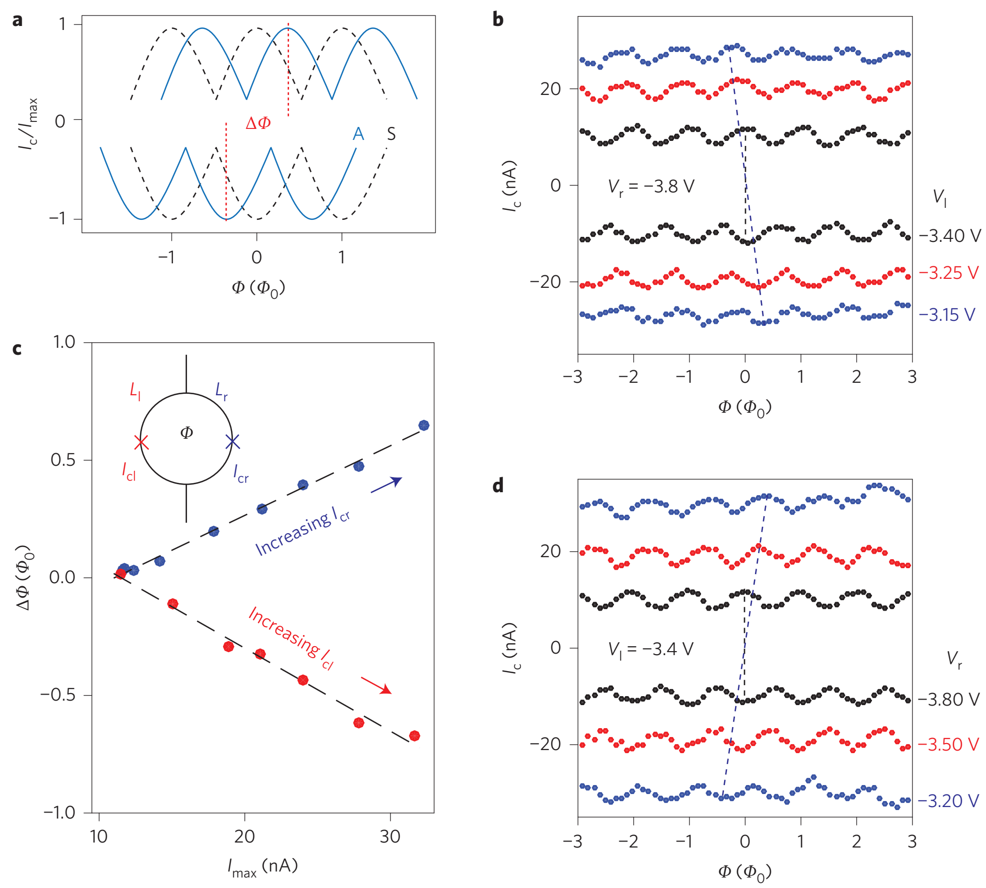

Figure 4 | Controllable asymmetry in E-SQUIDs. **a**, $I_c(\Phi)$ oscillations for a symmetric (S) SQUID (dashed black curve) and an asymmetric (A) SQUID with large L_k (solid blue curve). The maximum and minimum values of I_c shift along the Φ axis by $\Delta\Phi$. **b**, $I_c(\Phi)$ oscillations with V_r fixed and selected values of V_l. Black (blue) dashed line indicates the symmetric (asymmetric) configuration. **c**, Variation of $\Delta\Phi$ with I_{max} extracted from **b** and **d** but also including more values of the top gate voltage. The dashed lines show linear fits. Inset: Schematic of an asymmetric SQUID. **d**, $I_c(\Phi)$ oscillations for fixed V_l and varying V_r values.

the two arms of the SQUID loop (see ref. 28 for a description about asymmetric SQUIDs). The most important consequence of such asymmetry is that the $I_c(\Phi)$ curves are offset along the Φ axis (Fig. 4a). Such offsets arise due to the large L_k, which produces a substantial self-flux (Φ_s), in addition to the applied flux Φ. When the phase drop across each JJ reaches $\pi/2$, I_c reaches its maximal value $I_{max} = I_{cl} + I_{cr}$ and $\Phi_s(+) = I_{cr}L_r - I_{cl}L_l$. Reversing the direction of current bias results in the same magnitude of self flux, but now of the opposite sign (that is, $\Phi_s(-) = -\Phi_s(+)$.) Thus $\Delta\Phi = 2(I_{cr}L_r - I_{cl}L_l)$, where $\Delta\Phi = \Phi_s(+) - \Phi_s(-)$.

By controlling the two JJs in our E-SQUID we study the effects of such asymmetry in the SQUID response. In particular, we show that the ability to independently tune the critical current of each JJ gives us an alternative method to extract the kinetic inductance. We start with an electrostatic configuration identical to the one in Fig. 3c and plot $I_c(\Phi)$ (black curve in Fig. 4b). The black dashed line confirms that there are no discernible offsets on the Φ axis and the SQUID is in a symmetric configuration. We now hold V_r constant (and thus I_{cr} does not change) and make V_l less negative (increase I_{cl}). We find that the $I_c(\Phi)$ curves move towards the left (right) for positive (negative) current bias. The blue dashed line clearly indicates that $\Delta\Phi$ acquires a negative sign. Performing the same experiment with V_l fixed and opening the right gate, we expect I_{cr} to increase, thereby inducing a self-flux in the opposite direction. This sign reversal of $\Delta\Phi$ can be seen in Fig. 4d.

The variation of $\Delta\Phi$ with I_{max} is plotted in Fig. 4c. The blue (red) points correspond to measurements performed with V_r (V_l) varying while the other gate is fixed. As $\partial\Delta\Phi/\partial I_{cr} = 2L_r$ and $-(\partial\Delta\Phi/\partial I_{cl}) = 2L_l$, linear fits to these points (dashed lines) allow us to estimate $L_r \approx 31$ nH and $L_l \approx 36$ nH. This difference is within the error bars of our estimates and we conclude that any intrinsic asymmetry in the L_k values of the two arms is small. Thus, the observed shifts along the Φ axis arise from a combination of the large L_k and unequal critical currents of the JJs. This is a particularly important finding in the context of LAO/STO because it suggests that any mesoscopic inhomogeneities in the superfluid density[29,30] average out over a lengthscale of a few micrometres and do not have a considerable effect on the operation of these SQUIDs. Furthermore, even if such inhomogeneities are present, using the E-SQUID it is always possible to appropriately tune the critical current of the JJs to minimize the effects of self-flux.

The ability to probe the phase of the superconducting order parameter opens the door to answer more specific questions about the pairing symmetry. To do so, one could create more involved devices by combining the LAO/STO superconductor with an *s*-wave superconductor via JJs oriented along specific crystal axes[14]. From a technological perspective, our studies of the E-SQUID demonstrate the operation of a completely new variety of JJs that are both electrostatically defined and electrostatically controlled. Such an architecture for creating JJs eliminates any detrimental effects of the physical interfaces between dissimilar materials. Detailed transport spectroscopy studies should determine whether such electrostatic interfaces are in fact superior.

Received 11 December 2015; accepted 23 May 2016; published online 11 July 2016

References

1. Reyren, N. *et al.* Superconducting interfaces between insulating oxides. *Science* **317,** 1196–1199 (2007).
2. Caviglia, A. D. *et al.* Tunable Rashba spin-orbit interaction at oxide interfaces. *Phys. Rev. Lett.* **104,** 126803 (2010).
3. Ben Shalom, M. *et al.* Tuning spin-orbit coupling and superconductivity at the $LaAlO_3/SrTiO_3$ interface: a magnetotransport study. *Phys. Rev. Lett.* **104,** 126802 (2010).
4. Dikin, D. A. *et al.* Coexistence of superconductivity and ferromagnetism in two dimensions. *Phys. Rev. Lett.* **107,** 056802 (2011).
5. Bert, J. A. *et al.* Direct imaging of the coexistence of ferromagnetism and superconductivity at the $LaAlO_3/SrTiO_3$ interface. *Nature Phys.* **7,** 767–771 (2011).
6. Li, L. *et al.* Coexistence of magnetic order and two-dimensional superconductivity at $LaAlO_3/SrTiO_3$ interfaces. *Nature Phys.* **7,** 762–766 (2011).
7. Caviglia, A. D. *et al.* Electric field control of the $LaAlO_3/SrTiO_3$ interface ground state. *Nature* **456,** 624–627 (2008).
8. Richter, C. *et al.* Interface superconductor with gap behaviour like a high-temperature superconductor. *Nature* **502,** 528–531 (2013).
9. Ryazanov, V. V. *et al.* Coupling of two superconductors through a ferromagnet: evidence for a π junction. *Phys. Rev. Lett.* **86,** 2427–2430 (2001).
10. Weides, M. *et al.* 0-π Josephson tunnel junctions with ferromagnetic barrier. *Phys. Rev. Lett.* **97,** 247001 (2006).
11. Veldhorst, M. *et al.* Josephson supercurrent through a topological insulator surface state. *Nature Mater.* **11,** 417–421 (2012).
12. van Dam, J. A. *et al.* Supercurrent reversal in quantum dots. *Nature* **442,** 667–670 (2006).
13. Nelson, K. D. *et al.* Odd-parity superconductivity in Sr_2RuO_4. *Science* **306,** 1151–1154 (2004).
14. van Harlingen, D. J. Phase-sensitive tests of the symmetry of the pairing state in the high-temperature superconductors–evidence for $d_{x^2-y^2}$ symmetry. *Rev. Mod. Phys.* **67,** 515–535 (1995).
15. Cheng, G. *et al.* Electron pairing without superconductivity. *Nature* **521,** 196–199 (2015).
16. Takayanagi, H. & Kawakami, T. Superconducting proximity effect in the native inversion layer on InAs. *Phys. Rev. Lett.* **54,** 2449–2452 (1985).
17. Doh, Y.-J. *et al.* Tunable supercurrent through semiconductor nanowires. *Science* **309,** 272–275 (2005).
18. Heersche, H. B. *et al.* Bipolar supercurrent in graphene. *Nature* **446,** 56–59 (2007).
19. Brandt, E. H. & Clem, J. R. Superconducting thin rings with finite penetration depth. *Phys. Rev. B* **69,** 184509 (2004).
20. Khapaev, M. M. *et al.* Current distribution simulation for superconducting multi-layered structures. *Supercond. Sci. Technol.* **16,** 24 (2003).
21. Reyren, N. *et al.* Anisotropy of the superconducting transport properties of the $LaAlO_3/SrTiO_3$ interface. *Appl. Phys. Lett.* **94,** 112506 (2009).
22. Bert, J. A. *et al.* Gate-tuned superfluid density at the superconducting $LaAlO_3/SrTiO_3$ interface. *Phys. Rev. B* **86,** 060503 (2012).
23. McCollam, A. *et al.* Quantum oscillations and subband properties of the two-dimensional electron gas at the $LaAlO_3/SrTiO_3$ interface. *APL Mater.* **2,** 022102 (2014).
24. Tinkham, M. *Introduction to Superconductivity* 2nd edn (Dover, 1996).
25. Gallagher, P. *et al.* Gate-tunable superconducting weak link and quantum point contact spectroscopy on a strontium titanate surface. *Nature Phys.* **10,** 748–752 (2014).
26. Goswami, S. *et al.* Nanoscale electrostatic control of oxide interfaces. *Nano Lett.* **15,** 2627–2632 (2015).
27. Bal, V. V. *et al.* Gate-tunable superconducting weak link behavior in top-gated $LaAlO_3$-$SrTiO_3$. *Appl. Phys. Lett.* **106,** 212601 (2015).
28. Clarke, J. & Braginski, A. I. (eds) *The SQUID Handbook* Vol. 1 (Wiley, 2004).
29. Honig, M. *et al.* Local electrostatic imaging of striped domain order in $LaAlO_3/SrTiO_3$. *Nature Mater.* **12,** 1112–1118 (2013).
30. Kalisky, B. *et al.* Locally enhanced conductivity due to the tetragonal domain structure in $LaAlO_3/SrTiO_3$ heterointerfaces. *Nature Mater.* **12,** 1091–1095 (2013).

Acknowledgements

We thank T. Klapwijk, A. Geresdi, A. Akhmerov, A. Brinkman and J. Mannhart for useful discussions and feedback about the preliminary results. This work was supported by The Netherlands Organisation for Scientific Research (NWO/OCW) as part of the Frontiers of Nanoscience program, the Dutch Foundation for Fundamental Research on Matter (FOM), the Deutsche Forschungsgemeinschaft (DFG) via Project KO 1303/13-1 and EU-FP6-COST Action MP1308.

Author contributions

E.M. fabricated the devices. S.G. performed the transport measurements with help from E.M. S.G. and A.M.R.V.L.M. analysed the data. R.W., R.K. and D.K. carried out the numerical simulations and Y.M.B. provided theoretical support. L.M.K.V. and A.D.C. supervised the project. S.G. wrote the manuscript with input from all co-authors.

Additional information

Supplementary information is available in the online version of the paper. Reprints and permissions information is available online at www.nature.com/reprints. Correspondence and requests for materials should be addressed to S.G. and A.D.C.

Competing financial interests

The authors declare no competing financial interests.